

A theoretical investigation of the distribution of indoor radon concentrations

R Rabi and L Oufni*

Department of Physics (LPM-ERM), Faculty of Sciences and Techniques, Sultan Moulay Slimane University, B.P.523, 23000 Beni-Mellal, Morocco

Received: 13 December 2015 / Accepted: 03 October 2016 / Published online: 14 November 2016

Abstract: Inhalation of radon (^{222}Rn) and its decay products are a major source of natural radiation exposure. It is known from recent surveys in many countries that radon and its progeny contribute significantly to total inhalation dose and it is fairly established that radon when inhaled in large quantity causes lung disorder. In recent times, numerical modelling has become the cost effective replacement of experimental methods for the prediction and visualization of indoor pollutant distribution. The aim of this study is to implement the Finite Volume Method (FVM) for studying the radon distribution indoor. The findings show that the radon concentration which is distributed in a non-homogeneous way in the room is due to the difference in the radon concentration of different sources (wall, floor and ceiling). Moreover, the radon concentration is much larger near walls, and decreases in the middle of the room because of the effect of air velocity. We notice that the simulation results of radon concentration are in agreement with the results of other experimental studies. The annual effective dose of radon in the model room has been also investigated.

Keywords: Radon; Simulation; Finite Volume method; Ventilated room; Reynolds number; Radon effective dose

PACS Nos: 28.41.Te; 29.25.Rm; 07.05.Tp

List of symbols

c	Concentration of radon (Bqm^{-3})
c_i	Concentration of radon (Bqm^{-3}) in inlet
L	Height of the room (m)
p	Pressure (Nm^{-2})
Pr	Prandtl number
Sc	Schmidt number
Sh	Sherwood number
Nu	Nusselt number
Re	Reynolds number
Ra	Rayleigh number
Ri	Richardson number
Le	Lewis number
N	Buoyancy ratio
$\bar{\epsilon}_c$	Overall effectiveness coefficient for contaminant distribution
C_{average}	Average concentration of (^{222}Rn) inside the room (Bqm^{-3})
C_{outlet}	Average concentration of ^{222}Rn at the outlet (Bqm^{-3})

C_{inlet}	Average concentration of ^{222}Rn at the inlet (Bqm^{-3})
u	Velocity vector (ms^{-1})
w	Height of the opening (m)
x, y	Cartesian coordinates

Greeks symbols

ρ	Mixture density (Air- ^{222}Rn), Kg m^{-3}
λ	^{222}Rn decay constant (s^{-1})
D	Radon diffusivity in air ($\text{m}^{-2} \text{s}^{-1}$)
β_c	Thermal expansion coefficient, K^{-1}
g	Gravitational acceleration ($\text{m}^{-2} \text{s}^{-1}$)

1. Introduction

In the last few decades, significant interest in the harmful effect of radon on human health has been expressed. Most exposure to radon occurs indoors where it can accumulate due to poor ventilation [1–3]. This is ascribed to the fact that most building materials contain a certain amount of radium, which is a source of radon. When radium decays, the resulting atoms of radon gas escape from grains of the building material to air-filled pores and finally reach the

*Corresponding author, E-mail: oufni@usms.ma; loufni@gmail.com

room air by crossing the building material–air interface. Generally, inhalation of radon and its decay products in the indoor environment yields the greatest amount of the natural radiation exposure of humans. Nationwide measurements of radon activities in the indoor air of dwellings are continuously presented all over the world [4–6]. Interestingly, the numerous measurements of the concentrations of radon in different countries, along with the epidemiological studies, regarding the indoor radon and the risk of lung cancer, have been published during the recent years [7, 8]. Therefore, the estimation of the distribution of radon concentrations in the indoor air is very important for assessing the radiation dose received from the inhalation of radon and its progeny.

At present, limited experimental work has been reported on indoor radon [9]. The use of computer modelling for this application has been first reported by Jacobi [10] and Porstendorfer et al. [11]. However, these studies assumed a homogeneous distribution of radon concentration in the room. More recent studies [12, 13] have addressed this shortcoming, using numerical simulation. But, a major limitation of these studies is that they have not taken into

account the influences in the concentration of radon from different sources (wall, floor and ceiling).

In this work, the Finite Volume Method (FVM) has been used to simulate the radon concentrations distribution in the studied room. This model (FVM) simulates all relevant processes like diffusion, different kinds of ventilation, the concentration of radon from different sources (wall, floor and ceiling), convective air flow, radioactive decay, etc. A comparison of simulation results with other experimental data is also presented and the annual effective dose of radon in the room has been investigated.

2. Mathematical and physical model

2.1. Physical model of the ventilated room

The model of a ventilated room that we used to calculate the spatial distribution and concentrations of radon is shown in Fig. 1. It is a three-dimension, a full-scale room with a size of (4 m × 4 m × 4 m). The width of the inlet and outlet is *w* (1.0 m); and the inlet and the outlet are symmetrically placed about the center plane (*Z* = 2.0 m) [14], with the air inlet gap on the lower side of the left wall and the air outlet gap on the top of the right wall. Wall, floor and ceiling surfaces were taken as sources of radon; the inlet air velocity is a function of the Reynolds number (*Re*).

The in-room air flow was assumed to be steady-state, Newtonian and non-compressible in laminar regime, and the temperature inside the room was considered constant and uniform. With these considerations, the mass and momentum conservation equations are:

$$\frac{\partial u}{\partial x} + \frac{\partial v}{\partial y} + \frac{\partial w}{\partial z} = 0 \quad (1)$$

$$u \frac{\partial u}{\partial x} + v \frac{\partial u}{\partial y} + w \frac{\partial u}{\partial z} = -\frac{1}{\rho} \frac{\partial p}{\partial x} + \nu \left(\frac{\partial^2 u}{\partial x^2} + \frac{\partial^2 u}{\partial y^2} + \frac{\partial^2 u}{\partial z^2} \right) \quad (2)$$

$$u \frac{\partial v}{\partial x} + v \frac{\partial v}{\partial y} + w \frac{\partial v}{\partial z} = -\frac{1}{\rho} \frac{\partial p}{\partial y} + \nu \left(\frac{\partial^2 v}{\partial x^2} + \frac{\partial^2 v}{\partial y^2} + \frac{\partial^2 v}{\partial z^2} \right) + \beta_c (c - c_i) \quad (3)$$

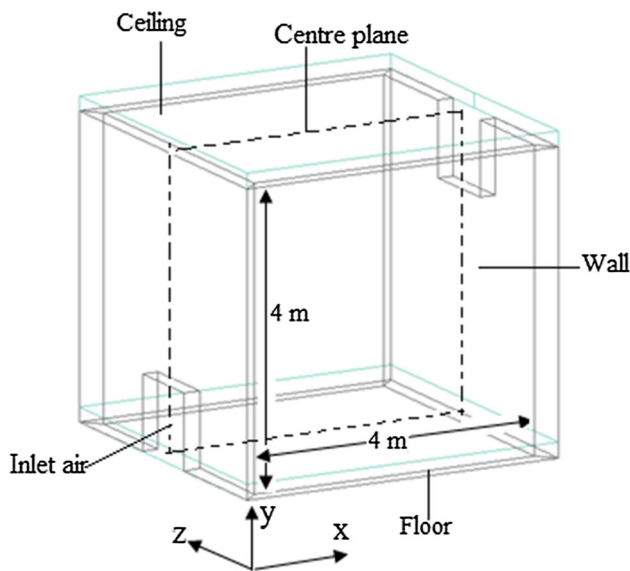


Fig. 1 Physical model for the studied ventilated room

Table 1 Walls, floor and ceiling constructions of the different room models [22]

Room models	Walls		Ceiling		Floor	
	Construction	Density (g cm ⁻³)	Construction	Density (g cm ⁻³)	Construction	Density (g cm ⁻³)
Model-1	Red Clay Bricks	1.1	Concrete	2.25	Concrete	177.60
Model-2	Cement layer	1.28	Gypsum layer	0.89	Ceramic	280.20
Model-3	Ceramic	1.35	Gypsum layer	0.89	Granite	456.90

Table 2 The uranium contents, radon alpha-activities in all building material samples [22]

	Concentration of ^{238}U (BqKg $^{-3}$)	Concentration of radon (Bqm $^{-3}$)
Gypsum layer	17.55	153.80
Cement layer	23.02	236.10
Red clay brick	30.98	146.60
Ceramic	49.52	280.20
Granite	51.36	456.90
Concrete	27.11	177.60

Table 3 Result of grid independence examination

Number of grids in X–Y	C_{average}	$\bar{\varepsilon}_c$
60 × 60	156.66	1.06
70 × 70	159.29	1.05
80 × 80	161.35	1.05
90 × 90	163.00	1.04

Table 4 Comparison of results obtained in this study by Corcione et al. [19]

Pr	Ra	Le	N	Corcione et al.		Present study		Error (%)
				Nu	Sh	Nu	Sh	
1.0	10 ⁴	1.0	0.50	1.77	1.77	1.76	1.76	0.37
10.0	10 ⁴	1.0	0.50	1.77	1.77	1.76	1.76	0.19
10.0	10 ⁶	1.0	0.50	7.65	7.65	7.65	7.56	0.00

Table 5 Comparison of results obtained in this study by Rahman et al. [20]

Pr	Ri	Re	Rahman et al.	Present study	Error (%)
<i>Percentage increase in average Nusselt number</i>					
0.71	2.0	100	1.92	1.96	2.11
0.71	1.0	100	1.82	1.90	7.29

$$u \frac{\partial w}{\partial x} + v \frac{\partial w}{\partial y} + w \frac{\partial w}{\partial z} = -\frac{1}{\rho} \frac{\partial p}{\partial z} + \nu \left(\frac{\partial^2 w}{\partial x^2} + \frac{\partial^2 w}{\partial y^2} + \frac{\partial^2 w}{\partial z^2} \right) \quad (4)$$

where: u , v and w are the Cartesian velocity components (m s $^{-1}$), p is pressure, ρ is mixture density (Air- ^{222}Rn), ν is the kinematic viscosity (m 2 s $^{-1}$), β_c is thermal expansion coefficient, c is radon concentration (Bqm $^{-3}$), and c_i is the radon concentration in inlet.

The dispersion of radon gas in the studied room was simulated using the following equation [15, 16]:

$$u \frac{\partial c}{\partial x} + v \frac{\partial c}{\partial y} + w \frac{\partial c}{\partial z} = D \left(\frac{\partial^2 c}{\partial x^2} + \frac{\partial^2 c}{\partial y^2} + \frac{\partial^2 c}{\partial z^2} \right) - \lambda c \quad (5)$$

where: c represents radon concentration in the room studied (Bqm $^{-3}$), D is the diffusion coefficient (m 2 s $^{-1}$), u , v and w are air flow velocity (m s $^{-1}$), λ is the radon decay constant (s $^{-1}$).

2.2. Boundary conditions

The boundary conditions for the velocity components: Velocities on all the wall surfaces are null. At the air inlet gap they are $u = u_i$, and at the outlet gap: the amount of air that enters into the room is equal to that which leaves the room. The boundary conditions for the concentration of radon: at the air inlet is considered null, and the walls are taken as source of radon. In this simulation, we suggest three room models differing on its wall, floor and ceiling construction materials, as given in Table 1. Construction materials and its characteristics are given for the three models in Table 2, and these room models are made of the cement layer which is a mixture of sand, cement and water that are commonly used in Morocco (e.g. 65% Sand and 35% cement). Ceiling and floor were represented by ceramic, granite, concrete and gypsum layer. Concrete was prepared in different mixtures of gravel, sand, cement and water that are commonly used in Morocco (e.g. concrete: 42% sand, 30% gravel and 28% cement, gypsum mixture: 85% gypsum and 15% white).

2.3. Numerical procedure

The above equations have been solved numerically based on the finite volume method using the SIMPLER algorithm in a staggered uniform grid system. A line-by-line tridiagonal matrix algorithm with relaxation has been used in conjunction with iterations to solve the nonlinear discretized equations. The convergence has been considered as reached when $\sum_{ij} |f_{ij}^{k+1} - f_{ij}^k| < 10^{-5} \sum_{ij} |f_{ij}^{k+1}|$, where f_{ij}^k stands for the value of u , v , p , c at the k th iteration level and grid location (i,j) in the plane (x, y) [17]. The numerical method was implemented in a FORTRAN software, and this non-commercial simulation code has been successfully employed to investigate coupled heat and mass transfer problems in media partially or fully filled up with porous material [18]. The accuracy of the numerical results is verified through numerous tests based on the grid size effect. A mesh independence study has been carried out with numerical meshes varying from 60 × 60 to 90 × 90 with 10-node increments on each axis. The discretization for the opaque wall is always 10 nodes on the horizontal direction for all the meshes. Shown in Table 3, a maximum deviation of 2.0% for the variables between

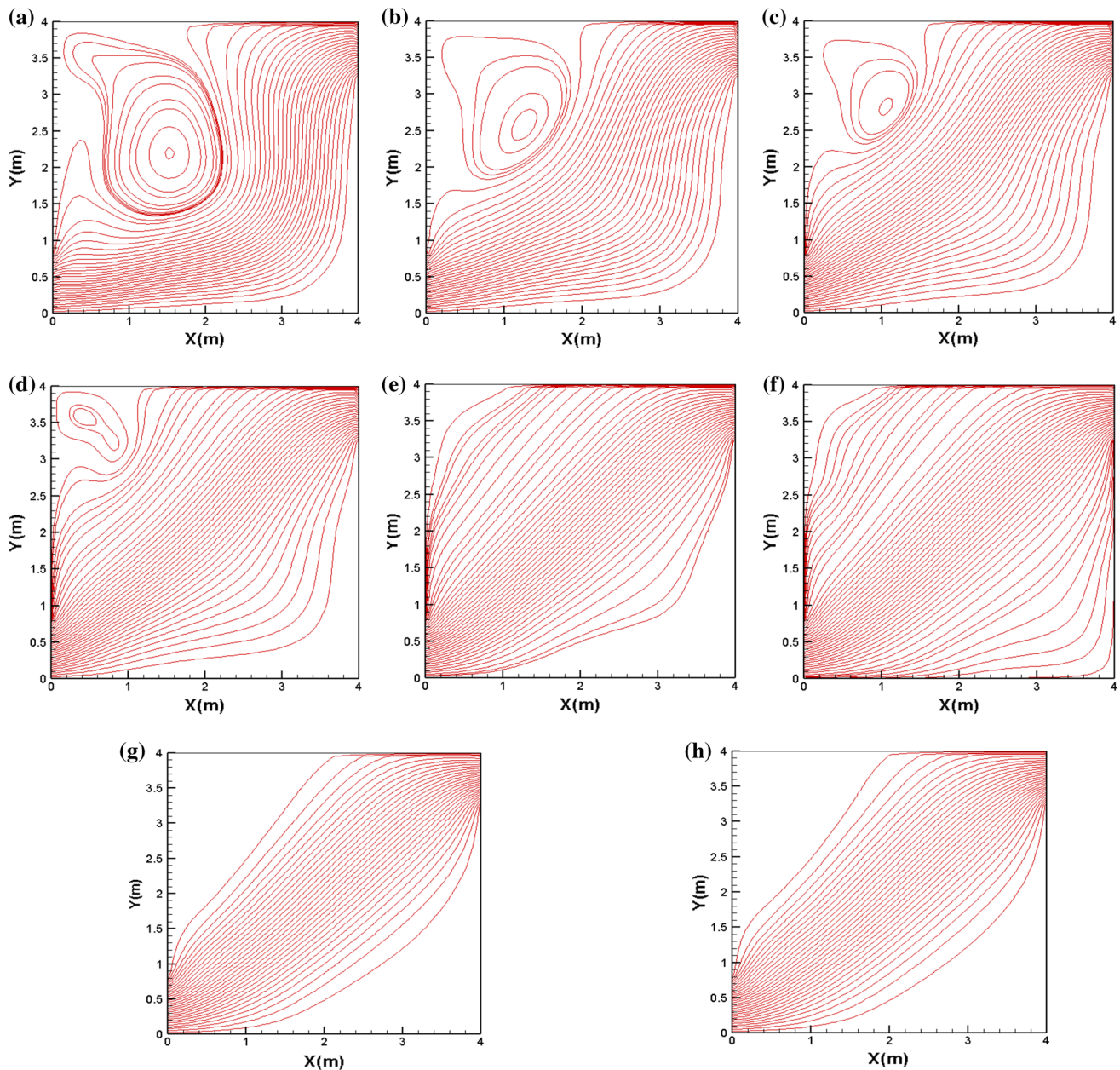


Fig. 2 Streamlines as a function of the Reynolds number in the ventilated room for the three studied models at symmetrical plane ($Z = 2.0$ m). (a) $Re = 10$, (b) $Re = 20$, (c) $Re = 50$, (d) $Re = 100$, (e) $Re = 500$, (f) $Re = 1000$, (g) $Re = 1500$ and (h) $Re = 2000$

meshes 60×60 and 90×90 has been observed. Therefore, an 80×80 grid was used in all cases considered herein.

A numerical code requires verification from the results reported in the literature or validated with experimental data. For this work, the lack of experimental data forced us to carry out verification for programming purposes, in order to obtain a reliable code. To validate our calculation code, we assumed that the decay term of radon, λ_c , (see Eq. 5) is equal to zero. Therefore, one finds the equation

used in the case of convection. To carry out verification, a problem involving double-diffusive natural convection in vertical square enclosures induced by opposite temperature and concentration gradients in horizontal direction is studied numerically by [19]. This comparison revealed good agreements between results as shown in Table 4. Another test for validation of this code has been performed in the case of vented square cavity; the results have been compared with those of [20] as shown in Table 5. From the above results, it can be concluded that

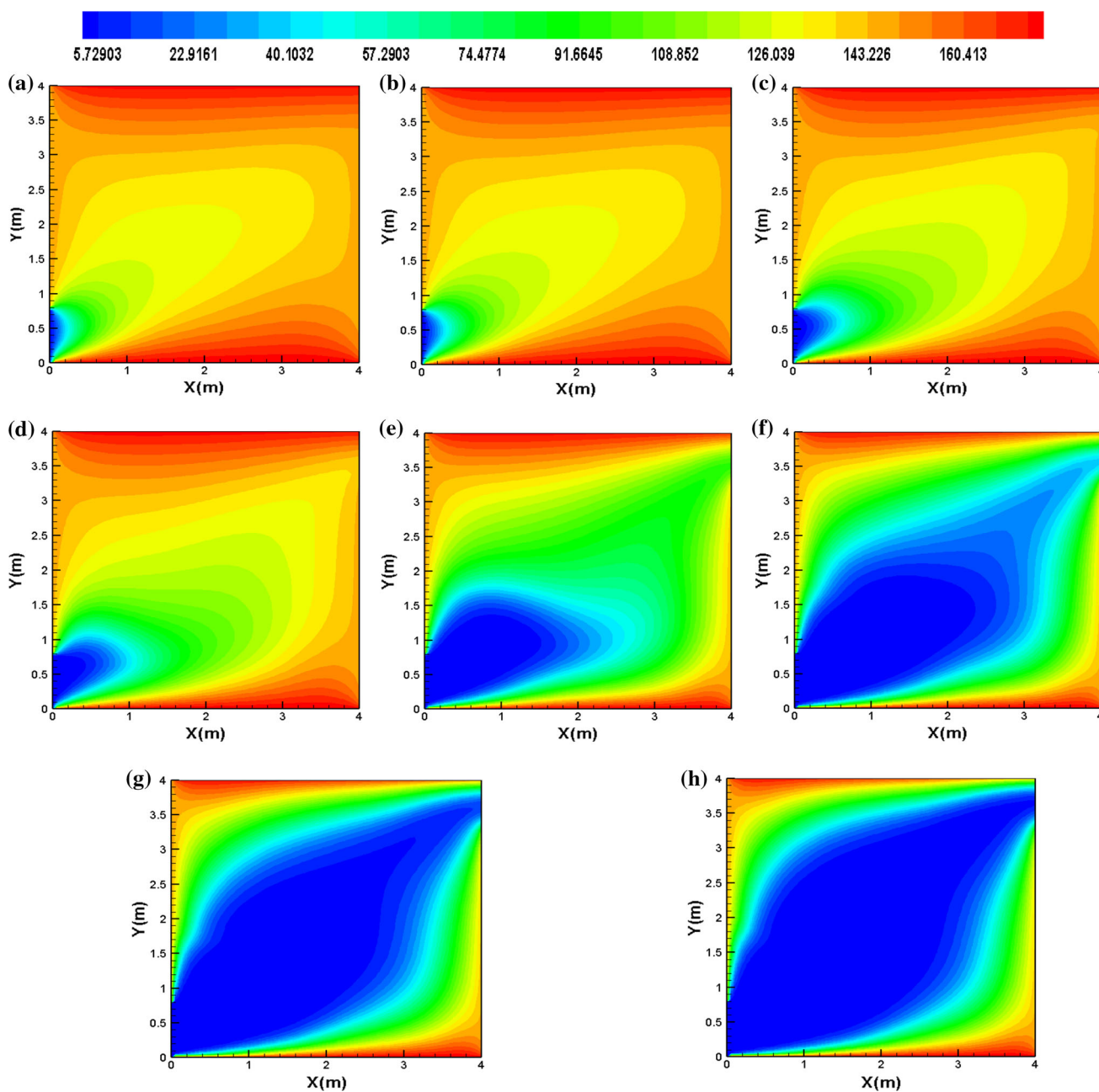


Fig. 3 Contours of radon concentration (Bqm^{-3}) as a function of different Reynolds number, Re , in the studied ventilated room for the studied model-1 at symmetrical plane ($Z = 2.0$ m). (a) $Re = 10$, (b) $Re = 20$, (c) $Re = 50$, (d) $Re = 100$, (e) $Re = 500$, (f) $Re = 1000$, (g) $Re = 1500$ and (h) $Re = 2000$

the numerical code, developed for this study shows satisfactory results.

3. Results and discussion

Numerical simulations were performed for the study of spatial distributions of radon in three models of the room, and at different Reynolds numbers. The Reynolds numbers

were calculated in the room using the equation $Re = \frac{u_0 w}{\nu}$, and were used as input for the FVM code. Our study was carried out for the interval $10 \leq Re \leq 2000$. Therefore, the indoor airflow may be regarded as laminar flow [12].

The effect of the Reynolds number on the flow structure is shown in Fig. 2(a)–(h). The three models represent the same streamlines because we have studied only one physical model for the ventilated room as shown in Fig. 1. For a jet imposed low intensity ($Re = 10$), Fig. 2(a) shows

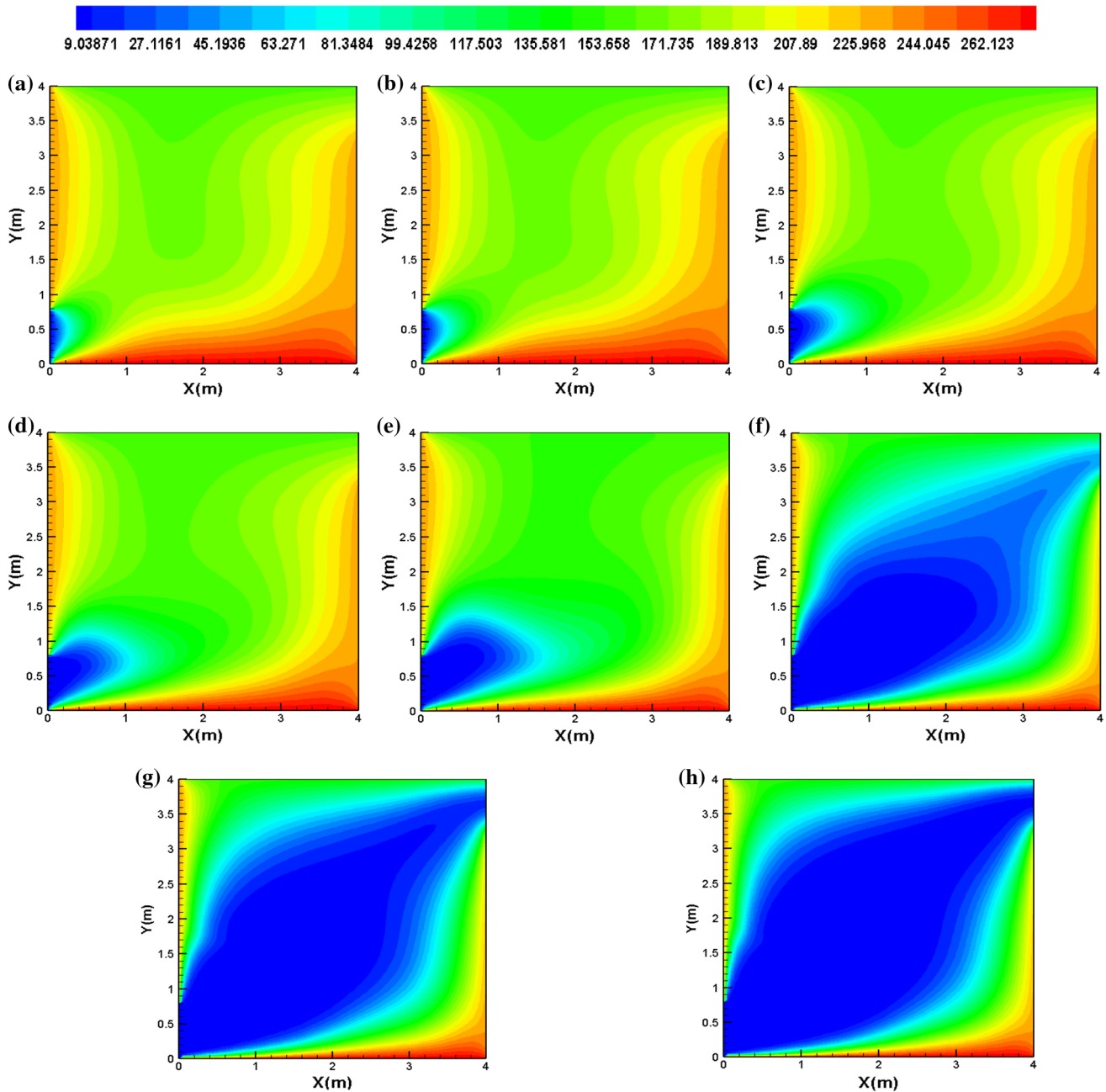


Fig. 4 Contours of radon concentration (Bqm^{-3}) as a function of different Reynolds number, Re , in the studied ventilated room for the studied model-2 at symmetrical plane ($Z = 2.0$ m). (a) $Re = 10$,

(b) $Re = 20$, (c) $Re = 50$, (d) $Re = 100$, (e) $Re = 500$, (f) $Re = 1000$, (g) $Re = 1500$ and (h) $Re = 2000$

that the presence of the convective cells constrains the majority of the open lines to describe an S trajectory before reaching the exit of the room. By increasing Reynolds number, the thickness of the open lines increases, which reduces the cell sizes as shown in Fig. 2(b)–(d). For $Re \geq 500$ (Fig. 2(e)–(g)), the convective cells disappear, and the open lines occupy nearly the entire room space. It is noted that for $Re = 2000$ (Fig. 2(h)), the forced flow crosses the room along the diagonal, which is due to the dominance of forced convection.

In order to investigate the spatial distribution of radon concentrations using FVM model, the contours of radon concentrations at the symmetrical plane ($Z = 2$ m) for different values of Reynolds number $Re = 10, 20, 50, 100, 500, 1000, 1500$ and 2000 , have been plotted and shown in Figs. 3, 4, 5. It was clearly observed that the radon concentration is distributed in a non-homogeneous way in the room, and this is due to the difference in the radon concentration of different sources (wall, floor and ceiling) (see Table 1). In general, for low values of the

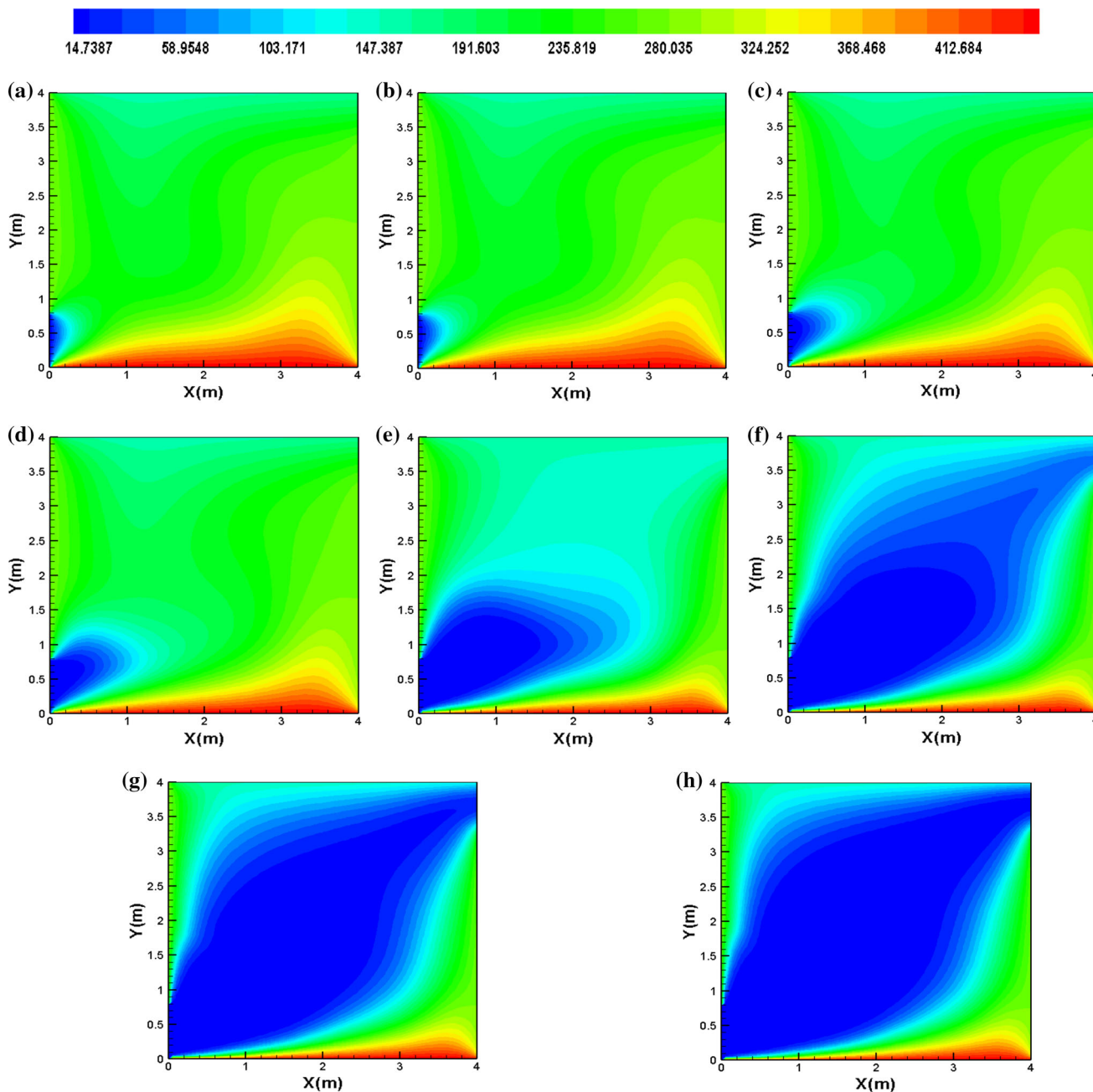


Fig. 5 Contours of radon concentration (Bqm^{-3}) as a function of different Reynolds number, Re , in the studied ventilated room for the studied model-3 at symmetrical plane ($Z = 2.0$ m). **(a)** $Re = 10$, **(b)** $Re = 20$, **(c)** $Re = 50$, **(d)** $Re = 100$, **(e)** $Re = 500$, **(f)** $Re = 1000$, **(g)** $Re = 1500$ and **(h)** $Re = 2000$

Reynolds number, we notice that the highest concentrations are obtained near the floor and the lowest values are close to the inlet. When the inlet velocity increases ($500 \leq Re \leq 2000$), the radon concentration decreases in the middle of the room, due to the effect of air velocity at the studied room. For $Re = 2000$, the concentration in the middle of the room will be about 40.0% smaller than that of the vicinity of the surface of the wall. We notice that the distribution of radon concentrations in a room depends

on the radon concentration of different sources (wall, floor and ceiling) and the ventilation; the latter can influence significantly radon measurement.

3.1. Average concentration inside the ventilated room

The geometric average concentration inside the room is given as [21]:

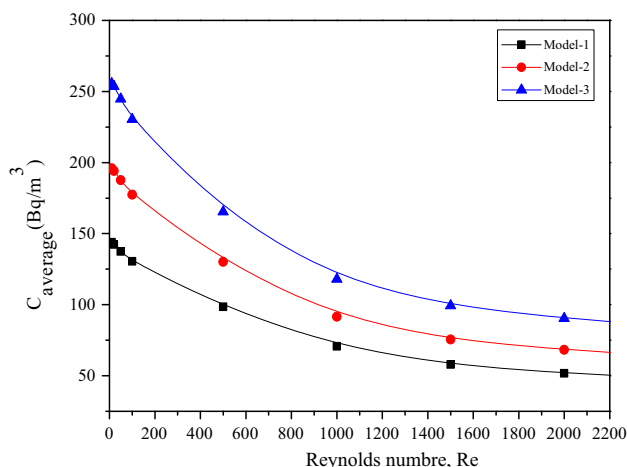


Fig. 6 Average ²²²Rn concentration in the room for 10 ≤ Re ≤ 2000

Table 6 Comparison of average concentration of ²²²Rn (Bqm⁻³) in the room results obtained in this study by Moharram et al. [22]

Room models	Moharram et al.	Present study	Error (%)
Model-1	40.41	47.93	18.61
Model-2	52.11	63.21	21.30
Model-3	73.53	84.61	15.07

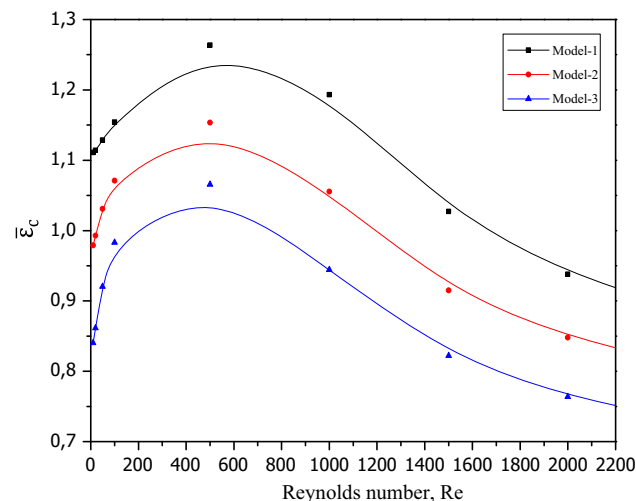


Fig. 7 Overall ventilation effectiveness for the removal of radon pollutants in the room for 10 ≤ Re ≤ 2000

$$C_{average} = \frac{\int \int c(x, y) dx dy}{\int \int dx dy} \tag{6}$$

Figure 6 shows the values of average concentration ($C_{average}$) inside the room as a function of the Reynolds number. From this figure, it can be seen that the pattern is

Table 7 Radon average concentration and annual effective doses (AED) calculated in the room

Room models	Average concentration of ²²² Rn indoor (Bqm ⁻³)	Annual effective doses (AED) (mSv y ⁻¹)
Model-1	47.93	1.51
Model-2	63.21	1.99
Model-3	84.61	2.66

similar for all models studied. The average concentration decreases when we increase the Reynolds number; model (3) shows the higher values of the ²²²Rn average concentration, and model (2) shows intermediate values. The maximum average concentration is obtained for Re = 10. When the ventilation rate is increased, the air change rate increases, which decreases the radon level.

As can be seen from Table 6, the results of the average values of the concentration of radon for Re = 2500 (equivalent to a ventilation rate of 0.5 h⁻¹) is compared with experimental results of Moharram et al. [22], closely (within 21.30% deviation). This validates the capability of the Finite Volume Method (FVM) for estimating the distribution of radon concentrations in dwellings.

3.2. Overall ventilation effectiveness for the removal of pollutants

The overall ventilation effectiveness for radon distribution $\bar{\epsilon}_c$, provides a quantitative index related to the way in which pollutants are distributed throughout the room. This parameter is expressed as:

$$\bar{\epsilon}_c = \frac{C_{outlet} - C_{inlet}}{C_{average} - C_{inlet}} \tag{7}$$

where: C_{outlet} = average concentration of ²²²Rn at the outlet. $C_{average}$ = average concentration of ²²²Rn all over the inside of the room. C_{inlet} = average concentration of ²²²Rn at the inlet.

Figure 7 shows the results for overall ventilation effectiveness as a function of the Reynolds number. For all models considered in this work, it can be seen from this figure that the highest rate of the distribution of radon concentrations is presented by model (3). The ventilation effectiveness rate reaches a maximum value for Re = 500, and later decreases. This value (Re = 500) corresponds to good ventilation in the room under study.

3.3. Estimation of in room radon concentration, exposure and annual effective dose

In order to estimate the Annual Effective Dose rate (AED), we have to take into account the conversion coefficient for

the absorbed dose and the indoor occupancy factor. In the UNSCEAR report [23], the committee used 9.0 nSv h^{-1} per Bqm^{-3} for the conversion factor (effective dose received by adults per unit ^{222}Rn activity per unit of air volume), 0.4 for the equilibrium factor of radon indoors and 0.8 for the indoor occupancy factor. Hence, the Annual Effective Dose rate (AED) in mSv y^{-1} is calculated by the following formula [24]:

$$\text{AED} = A_c(^{222}\text{Rn})D_fO_fE_f \times 24 \times 365 \times 10^{-6} \quad (8)$$

where $A_c(^{222}\text{Rn})$ is the measured ^{222}Rn activity (Bqm^{-3}), D_f is the dose conversion factor, O_f is the indoor occupancy, and E_f is the radon equilibrium factor indoors.

Table 7 shows the average concentration the radon in the room, ranged from 47.93 to 84.61 Bqm^{-3} in room models (1) and (3), respectively. The maximum indoor values were annual effective doses (AED) 2.66 mSv y^{-1} detected in the room Model (3) and the minimum indoor values were 1.51 mSv y^{-1} in the room Model (1). These values of radon effective dose are less than the maximum permissible dose defined by the annals of the International Commission on Radiological Protection (ICRP), which are about 10 mSv y^{-1} for occupational and public exposures [25].

4. Conclusions

A model based on the Finite Volume Method (FVM), for the simulation of radon distribution in a ventilated room, is studied in this paper. Using this model, it is possible to determine the radon distribution inside the room. It has been found that the distribution of radon concentrations is not the same everywhere due to the difference in the concentration from different source distribution (wall, floor and ceiling). Moreover, the radon concentration decreases in the middle of the room, because of the effect of air velocity at the studied room models. The simulation results of average concentration of the radon are compared with the results of other experimental studies. This study confirms that with increasing the ventilation rate, the radon concentration decreases, and we have found that the optimal ventilation value is obtained for $\text{Re} = 500$. From the simulation results, we conclude that model (1) is the most

appropriate model among the three to build a room. The ventilation is a good method for the radon dilution, as it helps to maintain the indoor air quality and decreases the radon concentration inside the room.

References

- [1] F Steinhausler *Environ. Intern.* **22** (Suppl. 1) S1111 (1996)
- [2] Q Guo, J Sun and W Zhuo *J. Nucl. Sci. Technol.* **37** 716 (2000)
- [3] K K Dwivedi et al. *Radiat. Meas.* **33** 7 (2001)
- [4] P C Deka, H Sarma, S Sarkar, T D Goswami and B K Sarma *Indian J. Phys.* **83** 1025 (2009)
- [5] M S Kandari and R C Ramola *Indian J. Phys.* **83** 1019 (2009)
- [6] R S Saini, M Nain, R P Chauhan, N Kishore and S K Chakravarti *Indian J. Phys.* **83** 1197 (2009)
- [7] F Bochicchio, F Forastiere, D Abeni and E Rapiti *Radiat. Protect. Dosim.* **78** 33 (1998)
- [8] R W Field et al. *Am. J. Epidemiol.* **151** 1091 (2000)
- [9] J Ma, H Yonehara, T Aoyama, M Doi, S Kobayashi and M Sakanoue *Health Phys.* **72** 86 (1997)
- [10] W Jacobi *Health Phys.* **22** 441 (1972)
- [11] J Postendorfer, A Wicke and A Schraub *Health Phys.* **34** 465 (1978)
- [12] W Zhuo, T Iida, J Moriizumi, T Aoyagi and I Takahashi *Radiat. Prot. Dosim.* **93** 357 (2001)
- [13] V Urosevic, D Nikezic, and S Vulovic *J. Environ. Radioact.* **99** 1829 (2008)
- [14] B Zhao and J Wu *J. Hazard. Mater.* **147** 439 (2007)
- [15] D Xie, H Wang and K J Kearfott *Atmos. Environ.* **60** 453 (2012)
- [16] K Akbari, J Mahmoudi and M Ghanbari *J. Environ. Radioact.* **116** 166 (2013)
- [17] H Elharfi, M Naïmi, M Lamsaadi, A Raji and M Hasnaoui *Int. Schol. Research Netw.* **2012** 16 (2012)
- [18] J A Rabi and A A Mohamad *Appl. Mathem. Modell.* **30** 1546 (2006)
- [19] M Corcione, S Grignaffini and A Quintino *Int. J. Heat Mass Transf.* **81** 811 (2015)
- [20] M M Rahman, M A Alim, M A H Mamun, M K Chowdhury and A K M S Islam *ARPJ. Eng. Appl. Sci.* **2** 2 (2007)
- [21] R S Kaluri and T Basak *Int. J. Heat Mass Transf.* **54** 2578 (2011)
- [22] B M Moharram, M N Suliman, N F Zahran, S E Shennawy and A R El Sayed *Annals of Nucl. Energ.* **45** 138 (2012)
- [23] UNSCEAR United Nations Scientific Committee on the Effects of Atomic Radiation. Sources, effects and risk of ionizing radiation (New York: United Nations) (2000)
- [24] L Oufni, M A Misdq and M Amrane *Radiat. Measur.* **40** 118 (2005)
- [25] International Commission on Radiological Protection, Proceedings of the Third International Symposium on the System of Radiological Protection. Annals of the ICRP **Vol 45** No. 1S (2016)